Ultrasound in Med. & Biol., Vol. 47, No. 6, pp. 1514–1527, 2021

0301-5629/$ - see front matter

https://doi.org/10.1016/j.ultrasmedbio.2021.02.004

● *Original Contribution*

RIGHT VENTRICULAR FLOW DYNAMICS IN DILATED RIGHT VENTRICLES: ENERGY LOSS ESTIMATION BASED ON BLOOD SPECKLE TRACKING ECHOCARDIOGRAPHY—A PILOT STUDY IN CHILDREN

Wadi Mawad,*,†,‡ Lasse Løvstakken,† Solveig Fadnes,† Thomas Grønli,† Patrick Segers,§ Luc Mertens,* and Siri Ann Nyrnes†,¶

* The Hospital for Sick Children, Toronto, Ontario, Canada; † Department of Circulation and Medical Imaging, Norwegian University of Science and Technology (NTNU), Trondheim, Norway; ‡ Department of Paediatrics, Montreal Children's Hospital, McGill University Health Centre, Montreal, Quebec, Canada; § Biommeda, University of Ghent, Ghent, Belgium; and ¶ Children's Clinic, St. Olav's University Hospital, Trondheim, Norway

(*Received* 14 *September* 2020; *revised* 24 *December* 2020; *in final from* 6 *February* 2021)

Abstract—Using blood speckle tracking (BST) based on high-frame-rate echocardiography (HFRE), we compared right ventricle (RV) flow dynamics in children with atrial septal defects (ASDs) and repaired tetralogy of Fallot (rTOF). Fifty-seven children with rTOF with severe pulmonary insufficiency (PI) (n = 21), large ASDs (n = 11) and healthy controls (CTL, n = 25) were included. Using a flow phantom, we studied the effects of imaging plane and smoothing parameters on 2-D energy loss (EL). RV diastolic EL was similar in ASD and rTOF, but both were greater than in CTL. Locations of high EL were similar in all groups in systole, occurring in the RV outflow tract and around the tricuspid valve leaflets in early diastole. An additional apical early diastolic area of EL was noted in rTOF, corresponding to colliding tricuspid inflow and PI. The flow phantom revealed that EL varied with imaging plane and smoothing settings but that the EL trend was preserved if kept consistent. (E-mail: wadi.mawad@mcgill.ca)

Key Words: **Blood flow imaging, Energy loss, Flow dynamics, Blood speckle tracking, High-frame-rate imaging.**

INTRODUCTION

Volume loading caused by a large atrial septal defect (ASD) or pulmonary insufficiency (PI) after tetralogy of Fallot repair (rTOF) results in right ventricle (RV) dilation. Although the RV is dilated in these two conditions, RV function generally remains preserved in ASD patients whereas progressive RV dysfunction can occur in rTOF patients (van der Ven et al. 2019). When RV longitudinal function is studied using strain imaging, RV longitudinal strain is typically reduced in rTOF patients but preserved or even increased in ASD patients (Dragulescu et al. 2013). Our group also reported that reduction in RV longitudinal function preferentially affects the RV apex in rTOF (Dragulescu et al. 2014). Right ventricular function is an important prognostic factor in patients with rTOF, and an early imaging biomarker anticipating later failure is still lacking. Disturbances in cardiac fluid dynamics and energetics are thought to precede morphologic changes (Pedrizzetti et al. 2015). Flow patterns within the left ventricle have been studied, mainly by cardiac magnetic resonance imaging (MRI) or particle imaging velocimetry echocardiography (echo-PIV) and, more recently, vector flow mapping (VFM) (Zhong et al. 2016; Nakashima et al. 2017). RV flow dynamics, however, have not been well characterized in humans. Four-dimensional-flow MRI has revealed increased RV vorticity in rTOF patients, compared with healthy controls (Hirtler et al. 2016). Energy-based descriptions of RV flow dynamics in rTOF have been proposed but have until recently relied on MRI and invasive pressure measurements (Fogel et al. 2012). With the use of VFM, energy loss (EL) was found to be predictive of RV function after tetralogy of Fallot repair (Shibata et al. 2018).

Recent advances in ultrasound technologies allow the study of cardiac fluid dynamics with a temporal resolution higher than ever before. A combination of high-

Address correspondence to: Wadi Mawad, B04.2656-1001 Décarie Boulevard, Montreal, QC, Canada H4 A3 J1. E-mail: wadi.mawad@mcgill.ca

frame-rate echocardiography (HFRE), obtained by plane wave imaging, with blood speckle tracking (BST) allows quantification of blood speckle velocities (Fadnes et al. 2017; Nyrnes et al. 2020), ultimately enabling direct quantification and visualization of blood flow vorticity and EL. The aim of this pilot study was to use blood speckle tracking to compare cardiac flow dynamics between patients with dilated RVs secondary to large ASD or PI after rTOF. To this end, we aimed to compare RV vorticity and to quantify and localize EL in both groups of volume-loaded RVs. To provide more insight into the practical use of the energy loss parameter, we further analyzed its sensitivity to positioning of the imaging plane and the effects of post-processing (smoothing) in a computer simulation model, as well as inter and intraobserver variability *in vivo*.

METHODS

Children with rTOF and severe PI, children with a large secundum ASD causing RV dilation (RV end-diastolic dimension Z score > 2.5) and healthy controls (CTL) from the Hospital for Sick Children in Toronto, Canada, and St. Olavs Hospital in Trondheim, Norway, between December 2015 and January 2018, were included. Consent from the parents of each participant was obtained before enrollment, as specified by the ethics review boards of both institutions (Toronto Hospital for Sick Children No. 1000050095; St. Olav's No. 2010/499). The upper age limit for inclusion was 10 y. Conventional echocardiographic parameters were obtained from clinical studies done immediately before the high-frame-rate acquisitions. RV three-chamber (RV3C) and four-chamber (RV4C) views were acquired using a modified Vivid E-9 system (GE Vingmed Ultrasound, Horten, Norway) with research software enabling high-frame-rate acquisitions using plane (unfocused) transmit beams and parallel receive beamforming (Nyrnes et al. 2020). The principle underlying our image acquisition is illustrated in Figure 1. At least three cardiac cycles were recorded with commercially available ultrasound probes, including the 6 S and 12 S phased-array probes (GE Healthcare, Milwaukee, WI, USA). Storage of IQ (in-phase and quadrature) data was required for the offline postprocessing and analysis with blood speckle tracking.

Validation and analysis of the energy loss measurement

To validate the EL measurement and analyze its sensitivity to changes related to imaging plane, as well as for data smoothing and dropouts, the 2-D EL was evaluated in a 3-D computer simulation as illustrated in Figure 2 (bottom left), mimicking the main flow events (filling, vortex formation and ejection) in a previously described ventricular model (Van Cauwenberge et al. 2016). This allowed for comparison with a known ground truth for both 2-D and 3-D velocity fields, with the flexibility to obtain standard and non-standard imaging views. We investigated the effect of small offsets ($\pm 5^\circ$) from the standard cardiac views on the 2-D EL values. Furthermore, we investigated the influence of dropouts and smoothing in the color Doppler and BST data on EL.

Energy-loss calculations and localization

The raw echo data obtained in patients and controls were transferred for offline analysis using in-house software developed for quantitative flow field analysis. The radial velocity measurement was derived from color Doppler, and the lateral velocity estimate was determined by speckle tracking (Wigen et al. 2018). For further analysis, the RV4C views needed to include the RV inlet and apex; the RV3C views needed to include the inlet, outlet and apex. Acquisitions with significant signal dropout were excluded. Quality of the acquisitions was assessed by two observers (SAN, SF), and only RV4C and RV3C views of good quality were analyzed. Segmentation of the flow field was performed by a single observer (WM). This was done to define the region of analysis and was achieved by delineating the endocardial border in both views. Systole and diastole were identified by closure and opening of the tricuspid valve. The first frame in which the tricuspid valve closed defined the start of systole, and the first frame in which the valve was open defined the start of diastole. By use of the measured velocities, EL in the 2-D plane was calculated from the RV4C view using the formula (Akiyama et al. 2017)

$$\mathrm{EL} = \mu \int 2\left(\frac{\partial v_x}{\partial x}\right)^2 + 2\left(\frac{\partial v_y}{\partial y}\right)^2 + \left(\frac{\partial v_x}{\partial y} + \frac{\partial v_y}{\partial x}\right)^2 dA \quad (1)$$

where $v = [v_x,\ v_y]$ is the blood velocity vector, $\mu = 0.004$ Pa · s is the blood viscosity, and dA indicates that the values are integrated over an area. The area of integration was in this work determined by the color flow image; that is, values were integrated where there is color flow signal for each frame. Temporal and spatial smoothing parameters were kept identical for all analyses (temporal smoothing = 40 ms, Gaussian spatial smoothing = 5×5 mm^2). The final energy loss values were calculated as the time-integrated values in systole and diastole, expressed in millijoules per meter. Vorticity (VO) quantifies the local rotation rate of blood in a

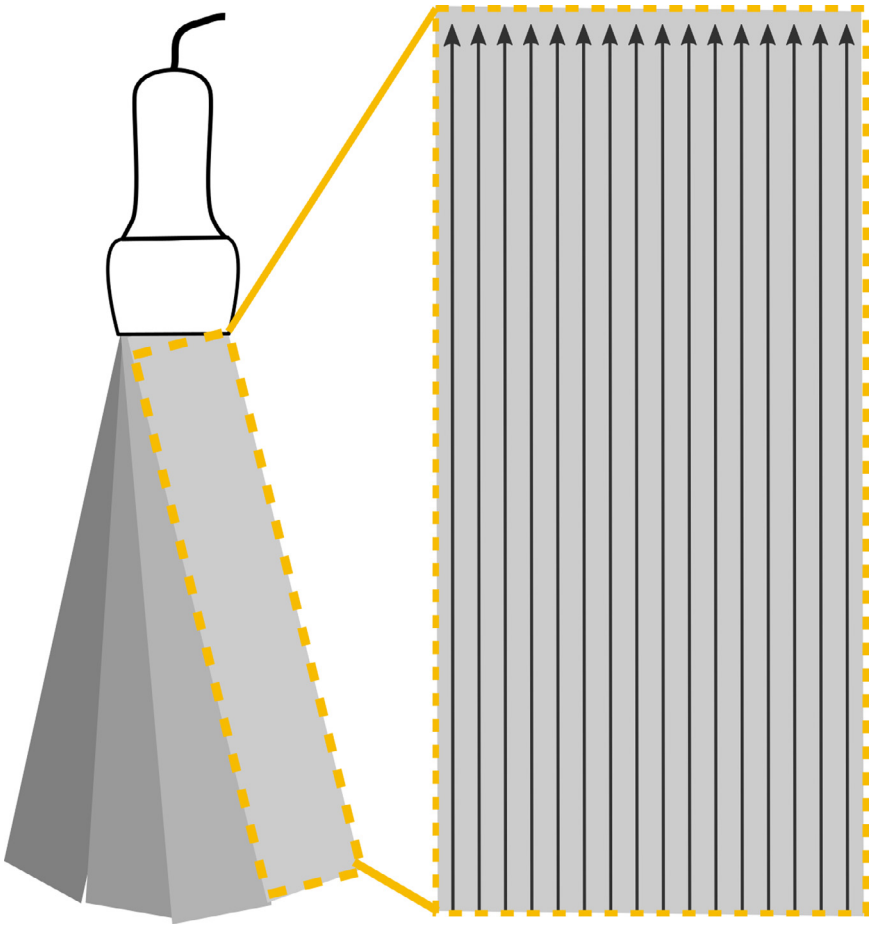

Fig. 1. Plane wave imaging and parallel receive beam forming. In this study, we used three to nine plane wave directions to cover the Doppler sector width. For each plane wave transmitted, multiple image lines (16 in our setup) were received simultaneously. Tracking can be done within the region covered by the 16 receive lines, where the frame rate equals the pulse repetition frequency.

2-D flow field. It was computed mathematically using the formula from the RV4C view and expressed in reciprocal seconds:

$$\mathrm{VO} = |\vec{\omega}| = \left| \frac{\partial v_y}{\partial x} - \frac{\partial v_x}{\partial y} \right| \quad (2)$$

An RV3C view was used to localize the areas of high EL because it provided simultaneous visualization of the RV inlet, apex and outlet flows in one 2-D cine loop. Only views including all three RV components were analyzed.

Reproducibility

A total of five randomly selected patients from each group were used to assess inter- and intra-observer variability in EL measurement from an RV4C view. We assessed this for EL only because both EL and VO rely on blood velocity measurements obtained with the same method. All the postprocessing analysis steps were repeated at an interval of 4 wk for the same observer and by a different observer (SAN). These were (i) definition of the timing points of systole and diastole as defined above; (ii) segmentation of a flow domain by tracing the endocardial surface of the RV; and (iii) calculation of EL in the selected cycle. For each patient, the same heart cycle in the RV4C cine loop was chosen by both observers, and all data were analyzed with the same smoothing settings.

Statistical analysis

Inter- and intra-observer analyses were assessed using Bland–Altman plots. Demographic and echocardiographic data were expressed as medians with quartiles (Q1–Q3). The Kruskal–Wallis test was used to test the differences in energy losses in three groups (CTL, rTOF and ASD). Comparison between two groups was done using the Mann–Whitney *U*-test, where a p value < 0.05 was considered to indicate statistical significance.

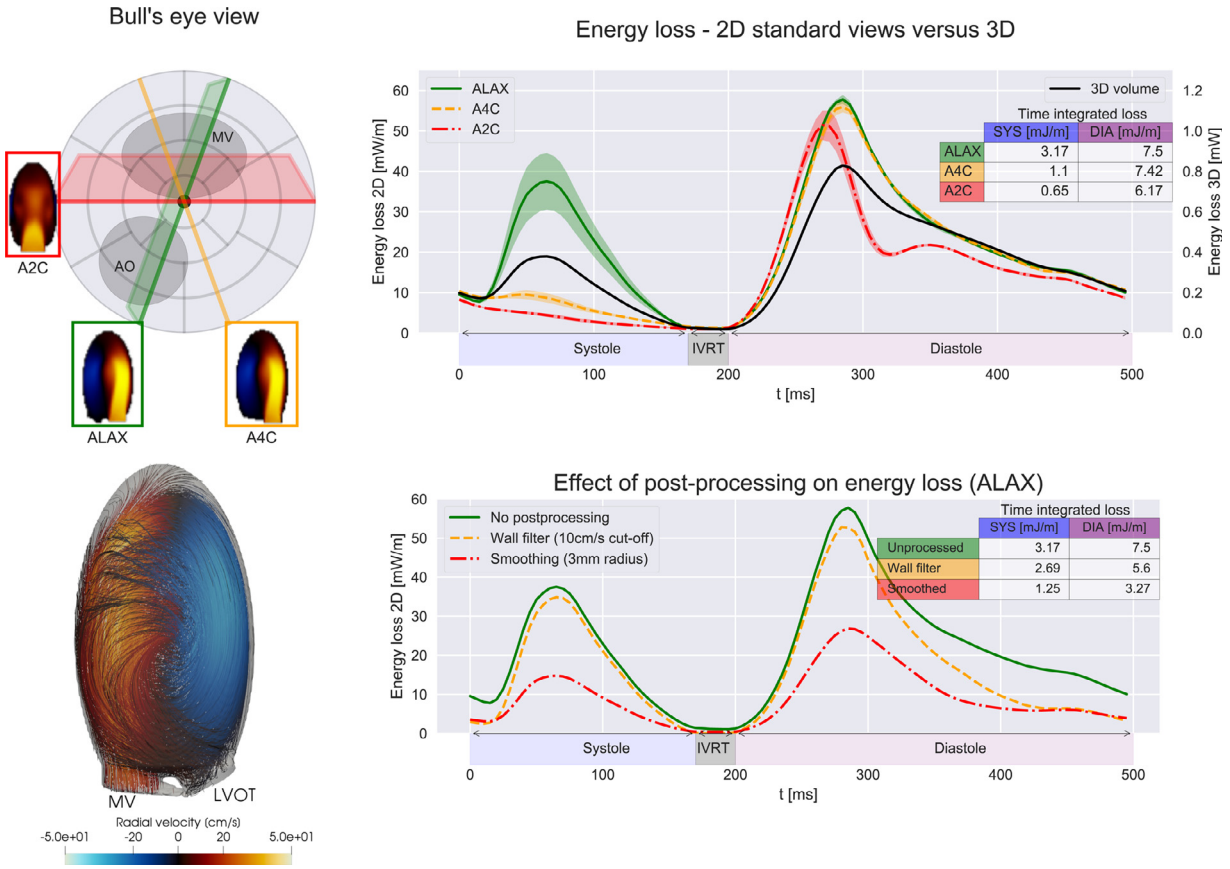

Fig. 2. Analysis of the energy loss metric in a computer simulation model mimicking 3-D ventricular flow. Bottom left: Snapshot of the flow pattern in the model in late diastole. In the Upper left: Bull's-eye view marking the mitral valve and outflow tract of the phantom along with the imaging plane/position of the selected standard examination views. Top right: The energy losses for standard views are traced along with variation resulting from the ±5° change in angle in the shaded lines. Little variation is noted in diastole, with some more important variations in systole from the ALAX view. Bottom right: The influence of the estimated values after postprocessing operations is plotted for the ALAX view with varying degrees of smoothing parameters. This indicates that increasing spatial smoothing reduces the EL magnitude but retains the curve shape (*red dotted line*). Wall filtering (*yellow line*) has little effect on EL magnitude and curve shape. ALAX = apical long axis; A2C = apical two-chamber; A4C = apical four-chamber; DIA = diastolic; EL = energy loss; IVRT = isovolumic relaxation time; LVOT = left ventricle outflow tract; MV = mitral valve; SYS = systole.

Correlations were tested using Spearman's rank test. The analyses were conducted using GraphPad Prism 8 (GraphPad Software, San Diego, CA, USA).

RESULTS

Validation and analysis of EL calculations using CFD

The computer-simulated validation and analysis of the EL measure are summarized in Figure 2. Our first aim was to evaluate how closely the 2-D EL for standard views compares with the true 3-D EL and to investigate how deviations from these imaging planes influence the 2-D EL measurement.

The 3-D EL curve indicates that most energy loss in the model occurs in diastole, where the filling jet leads to vortex formation with added shearing fluid losses. For the standard 2-D views, both the apical long-axis (ALAX) and apical four-chamber (A4C) views provided a fair representation of the diastolic 3-D EL (relative error: ±5% and ±4%, respectively). These 2-D views had similar integrated EL values with limited sensitivity to imaging view alignment (Fig. 2, upper right panel, *shaded color regions* around the curves). The apical two-chamber view (A2C), however, had the highest error (±9%). For systole, both the EL traces and integrated values varied substantially among imaging planes (relative error ALAX: ±19%, A4C: ±13%, A2C: ±17%). These findings supported the use of A4C views in our patients in diastole.

Our second aim was to analyze the influence of changes in postprocessing on the estimated 2-D EL and is shown for the ALAX view in Figure 2 (lower right plot). It can be observed that (i) spatial smoothing reduces EL magnitude but retains the curve shape, and (ii) the wall

filter has little influence in systole but may lead to some underestimation of EL in mid-to-late diastole.

To summarize, the computer simulation EL analysis revealed that, first, 2-D diastolic EL measures from A4C and ALAX views agree well with the 3-D EL shape, and the 2-D systolic EL measure from the ALAX view agrees well with the 3-D EL shape. Second, the effect of postprocessing is mainly a change in EL magnitude and can be used to compare relative changes. Consistent postprocessing parameters should be used, and clear baseline values should be provided.

RV energy loss calculations in TOF and ASD patients

In total, 21 rTOF (16 had received a transannular patch repair, 5 with an RV-to-pulmonary artery conduit), 11 ASD and 25 control patients were included, all with a suitable RV4C view for analysis. All rTOF patients had severe PI and no residual right ventricular outflow tract obstruction. The RV3C view was suitable (defined as a loop including high-quality BST measurements in the inflow, outflow and apex) only in 11 of 25 controls, 9 of 11 patients with ASD and 15 of 21 patients with rTOF.

Baseline demographic characteristics were similar among the three groups (Table 1). QRS duration was longer in the rTOF group compared with the other groups. When echocardiographic parameters of RV size and function were compared, the RVs were enlarged in ASD and rTOF patients compared with controls. Although RV fractional area change (FAC) was similar among the three groups, tricuspid annular plane systolic excursion (TAPSE) was significantly lower in the rTOF group compared with the other groups, whereas it was higher in the ASD patients compared with the other groups (Table 2). Tricuspid early diastolic inflow velocity (TVE) did not significantly differ among the groups. Left ventricular (LV) systolic function parameters did not significantly differ among the three groups.

Quantitative results from RV four-chamber views

Table 2 and Figure 3 compare the flow characteristics among the three groups as derived from blood speckle tracking. Compared with the CTL group, both the ASD and rTOF groups had significantly higher diastolic EL. Systolic EL, on the other hand, was similar in all groups. Diastolic vorticity was also significantly higher in ASD and rTOF as compared with CTL, whereas maximal systolic vorticity was similar in all groups. No significant correlation of heart rate, BSA or QRS duration with EL or vorticity was noted in any group. There were weak statistically significant correlations of systolic and diastolic EL with age in rTOF and CTL but not in ASD, with a wide spread of values as age increased. Energy loss and vorticity did not correlate with any conventional RV functional parameter.

Qualitative results from RV three-chamber views

When localizing regions of highest EL from the RV3C, all groups had a similar region of high systolic EL (Supplementary Videos S1, S2 and S3 [online only] for CTL, ASD and rTOF, respectively) and VO (Supplementary Videos S4, S5 and S6 [online only] for CTL, ASD and rTOF, respectively) in the right ventricular outflow tract. In diastole, all groups had high EL and VO around the tricuspid valve leaflets, corresponding to

Table 1. Demographic and echocardiographic data

	CTL (n = 25)	rTOF (n = 21)	ASD (n = 11)
Age (mo)	42 (26–76)	41 (21–74)	66 (33–99)
Male (%)	48%	52%	54%
Height (cm)	100 (85–124)	95 (82–109)	104 (88–134)
Weight (kg)	15.8 (12.3–23.6)	12.2 (10.0–19.5)	17.9 (10.5–27.3)
$BSA_{Haycock}$ (m^2)	0.94 (54–1.2)	0.84 (0.69–1.03)	0.74 (0.50–1.00)
Heart rate (bpm)	97 (85–108)	93 (85–100)	97 (89–101)
QRS duration (ms)	81 (77–93)	114 (80–128)*	82 (72–92)†
RV EDd (mm)	13 (10–16)	19 (17–23)	25 (21–32)
RV EDd Z-score	−0.4 (−1.4 to 0.9)	3.3 (2.7–3.5)*	4.6 (2.8–5.1)*
TAPSE (mm)	20 (18–23)	11 (10–13)*	23 (17–27)*,†
RV diastolic area (cm^2)	9.0 (7.6–13.3)	15.2 (8.8–17.6)*	18.2 (14.2–20.3)*,†
RV systolic area (cm^2)	5.6 (4.0–7.7)	8.7 (5.9–10.7)*	14.1 (10.5–20.3)*
RV FAC (%)	40 (37–46)	37 (33–42)	45 (37–48)
TV E (cm/s)	84 (72–126)	84 (71–100)	80 (70–101)
LV ejection fraction (%)	69 (64–74)	64 (61–68)	66 (61–70)
LV shortening fraction (%)	36 (32–39)	34 (32–37)	35 (31–38)

ASD = atrial septal defect; BSA = body surface area; CTL = controls; EDd = end-diastolic dimension; FAC = fractional area change; LV = left ventricle; RV = right ventricle; rTOF = repaired tetralogy of Fallot; TAPSE = tricuspid annular plane systolic excursion; TV E = tricuspid valve E-wave velocity.

Values are expressed as the median (quartiles Q1–Q3).

* p value < 0.05 versus CTL.

† p value < 0.05 versus rTOF.

Table 2. Right ventricular energy loss and vorticity in the four-chamber view

	CTL (n = 25)	rTOF (n = 21)	ASD (n = 11)
Systolic energy loss (mJ/m)	0.17 (0.10–0.48)	0.29 (0.07–0.51)	0.44 (0.29–0.68)
Diastolic energy loss (mJ/m)	1.34 (0.55–2.06)	1.93 (1.46–2.74)*	2.86 (1.47–3.65)*
Maximal systolic vorticity (1/s)	3.66 (2.02–5.98)	6.57 (1.52–11.19)	13.90 (6.13–18.41)
Maximal diastolic vorticity (1/s)	14.09 (8.36–17.61)	23.01 (17.73–28.52)*	28.74 (21.55–33.80)*

ASD = atrial septal defect; CTL = controls; rTOF = repaired tetralogy of Fallot.
Values are expressed as the median (quartiles Q1–Q3).
p-value < 0.05: *ASD or rTOF versus CTL.

vortex formation at the edge of the tricuspid valve leaflets. In rTOF, however, an additional region of high EL and VO was present in most cases (11/15) in the RV apex, corresponding to colliding PI and tricuspid inflow. Cardiac blood speckle tracking findings are summarized in schematic form in Figure 4 and in typical examples in Figure 5. The systolic and diastolic flow patterns were similar in CTL (Supplementary Video S7, online only) and ASD (Supplementary Video S8, online only), with diastolic vortices forming around the tricuspid valve leaflets in early diastole and accentuated with atrial systole followed by streaming toward the right ventricular outflow tract. In rTOF, systolic flow patterns were also similar to those of the other groups, but in diastole,

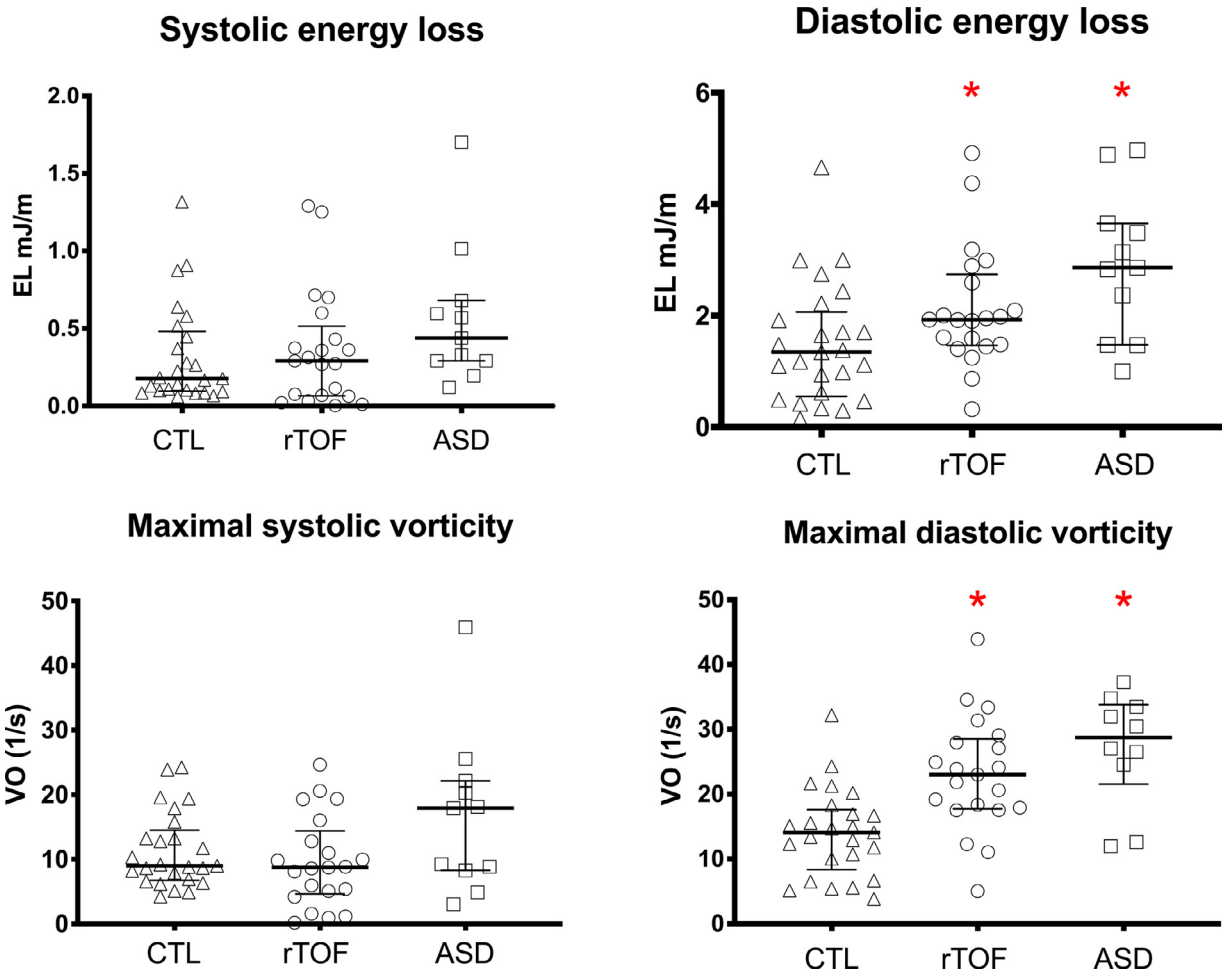

Fig. 3. Scatterplot of right ventricular flow energetics in the four-chamber view. Scatterplots of energy loss and vorticity with median (*thick line*) and quartiles (Q1–Q3, *thin line*). ASD = atrial septal defect; CTL = controls; EL = energy loss; rTOF = repaired tetralogy of Fallot; VO = vorticity. *p Value < 0.05, ASD or rTOF versus CTL. †p Value < 0.05, rTOF versus ASD.

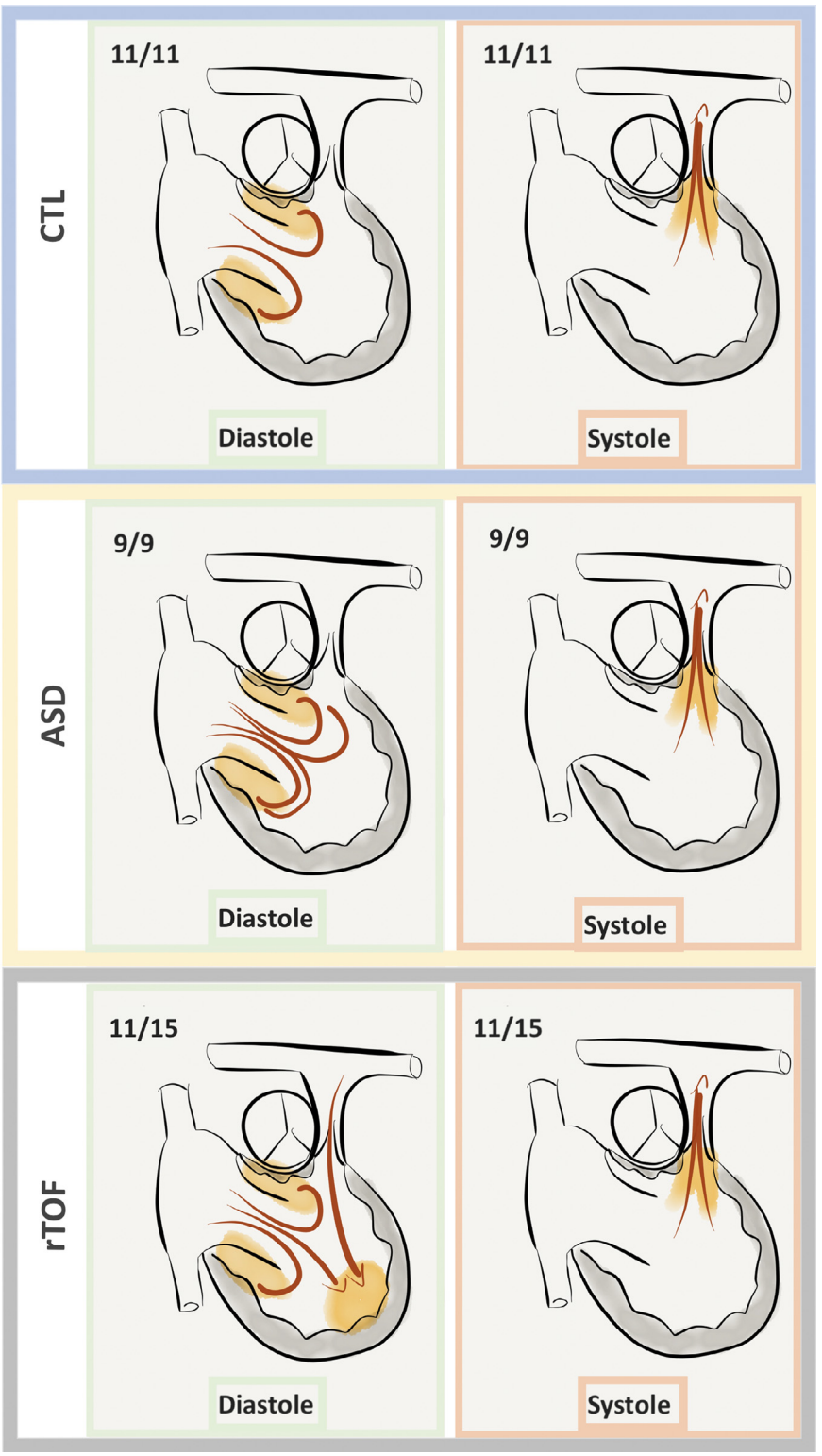

Fig. 4. Schematic of regions of high energy loss (*yellow shadowed areas*) as seen in the right ventricular three-chamber view. ASD = atrial septal defect; CTL = controls; rTOF = repaired tetralogy of Fallot.

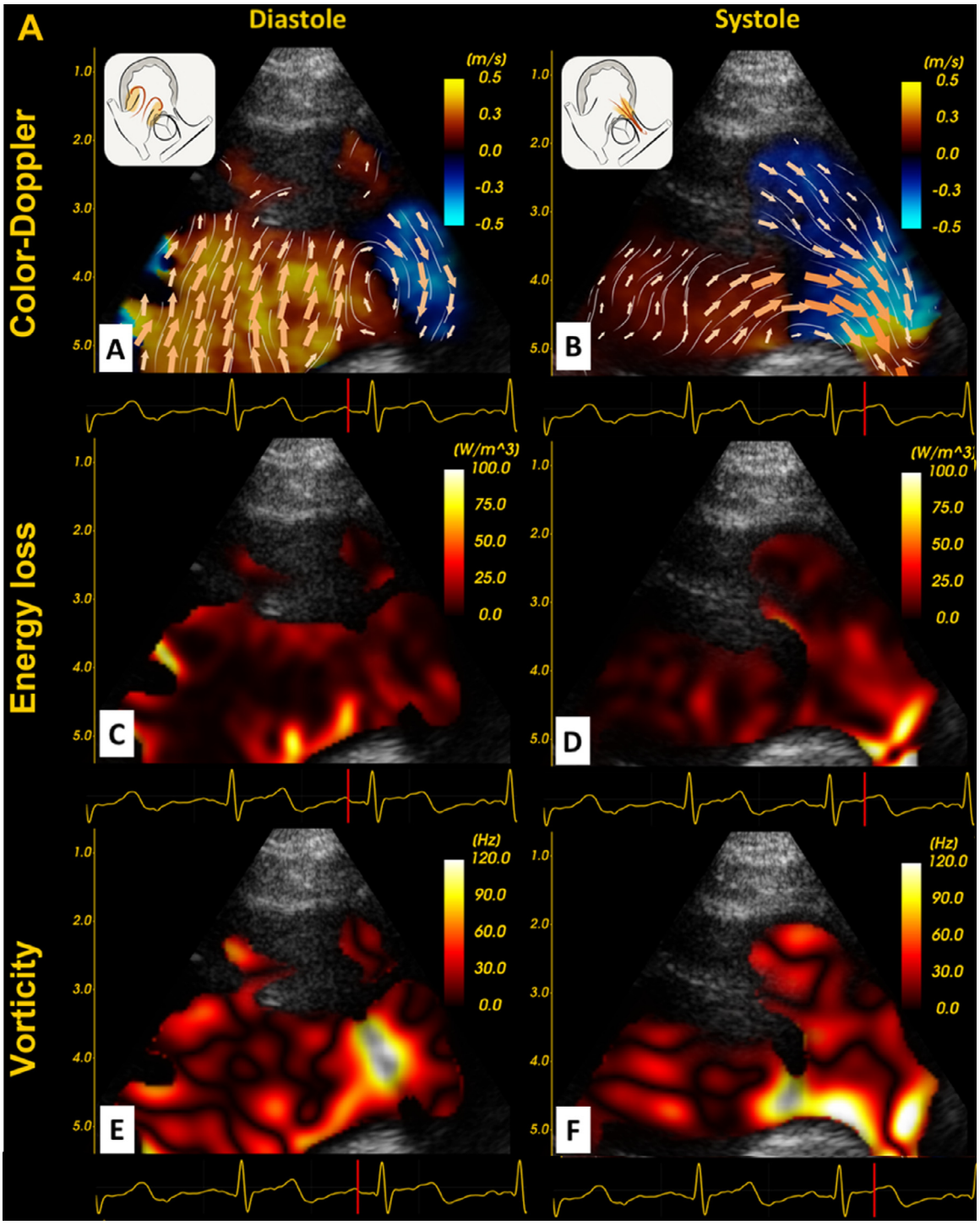

Fig. 5. Typical examples of right ventricle intracardiac velocities, energy loss and vorticity mapping in diastole and systole in controls (5A), patients with atrial septal defect (ASD) (5B) and patients with repaired tetralogy of Fallot (rTOF) (5C). The systolic and diastolic flow patterns were similar in CTL and ASD, with diastolic vortices forming around the tricuspid valve leaflets in early diastole (A and B, panel A) with corresponding areas of high energy loss and vorticity (A and B, panels C−E). In rTOF, systolic flow patterns were also similar to those of the other groups (A− C, panel B), but in diastole, regurgitant pulmonary flow collides with the tricuspid inflow, resulting in disorganized apical vortices (C, panel A, indicated by *white arrow*) with an additional area apical energy loss and vorticity (C, panels C and D, indicated by *white arrow*). The schematic in the upper left of each panel illustrates the imaging plane and areas of high EL in *orange.*

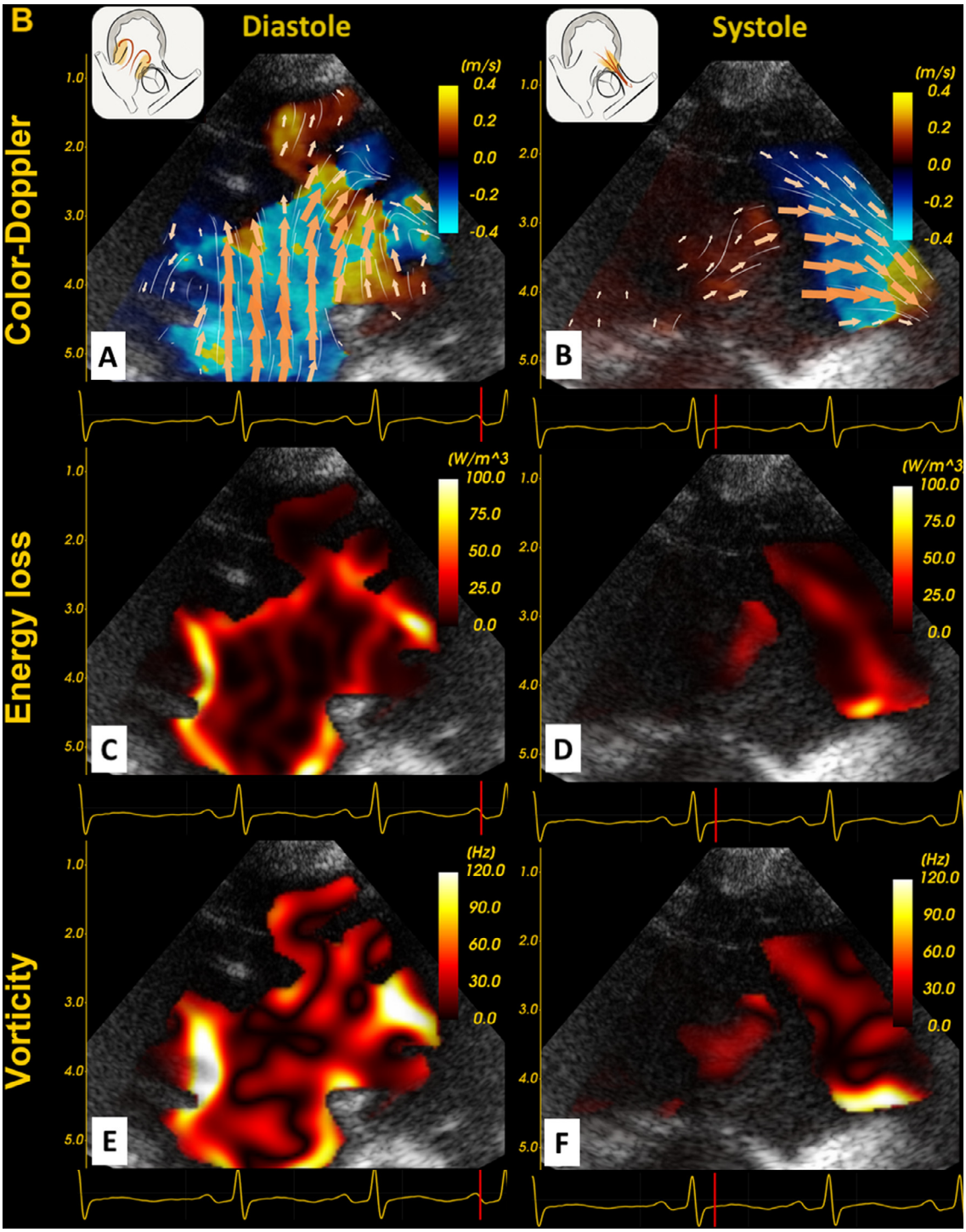

Fig. 5. Continued

regurgitant pulmonary flow collides with the tricuspid inflow, resulting in disorganized apical vortices (Supplementary Video S9, online only). The pattern of EL could also vary from beat to beat, as illustrated in Figure 6.

Inter- and intra-observer variability

Analysis of intra-observer variability revealed very good reproducibility for both diastolic and systolic EL measurements, with average systematic measurement

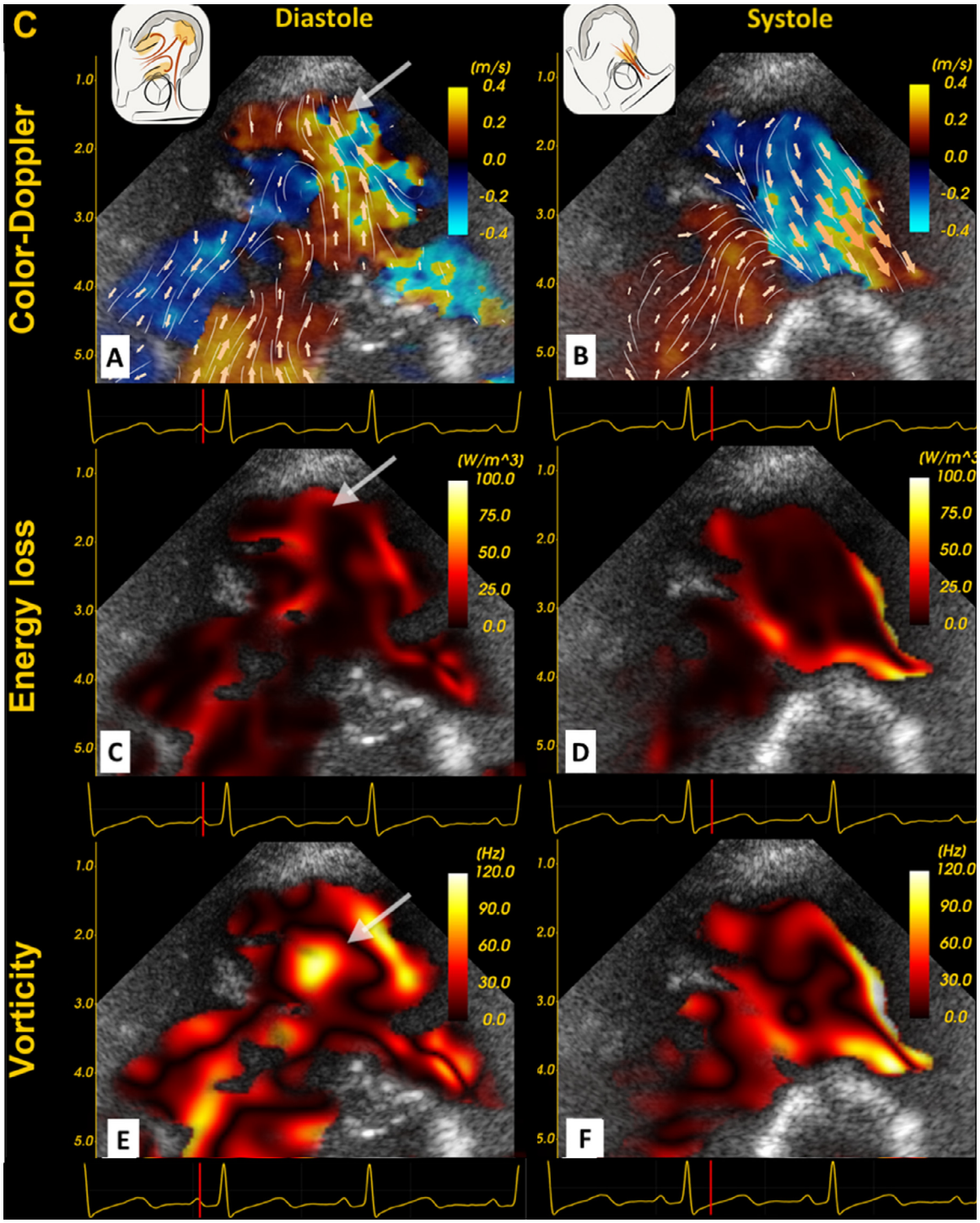

Fig. 5. Continued

errors of −0.1% and 0.0%, respectively, and very narrow limits of agreement, well within 5% variation. Analysis of inter-observer variability also revealed good reproducibility for both diastolic and systolic EL, with an average systematic error of 0.0% for both parameters and a narrow limit of agreement within 5% variation from the RV4C view (Fig. 7). The inter- and intra-observer variability was not determined for the RV3C view because this served to supply a qualitative measure, although findings were reviewed by co-authors (WM, SAN, LL, SF).

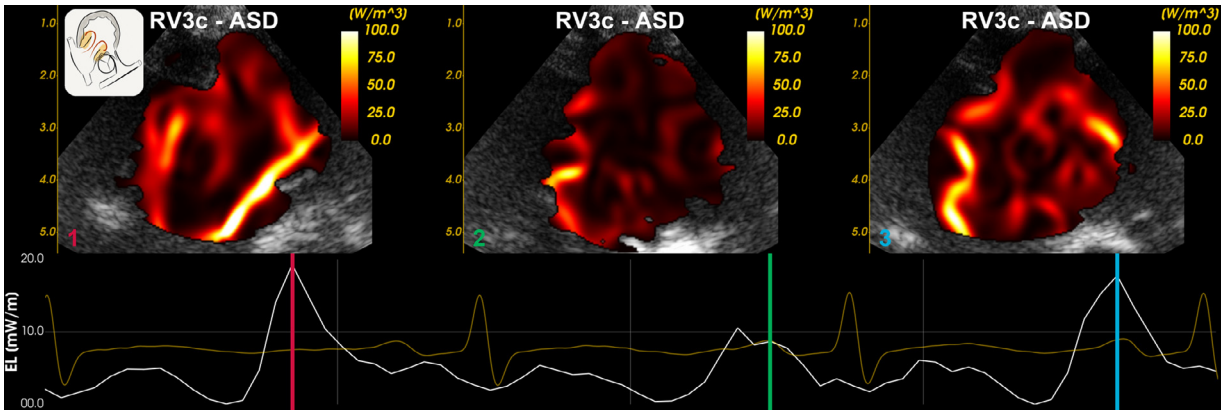

Fig. 6. Beat-to-beat variation of energy loss patterns. Energy loss mapping from a right ventricle three-chamber view revealing different patterns of energy loss from beat to beat in an example of a patient with ASD. RV3C = right ventricular three-chamber view; ASD = atrial septal defect.

DISCUSSION

In this study we compared cardiac blood flow energy losses between two groups with volume-loaded RVs and controls using high-frame-rate ultrasound imaging and blood speckle tracking. We studied the feasibility and reproducibility of blood speckle tracking and validated energy loss measurements. We described different blood flow dynamics and energetics in volume-loaded RVs compared with controls.

Although the EL parameter varied for different patient groups, it could also vary substantially because of changes in image plane and postprocessing (smoothing). Beat-to-beat variation in EL patterns could also be

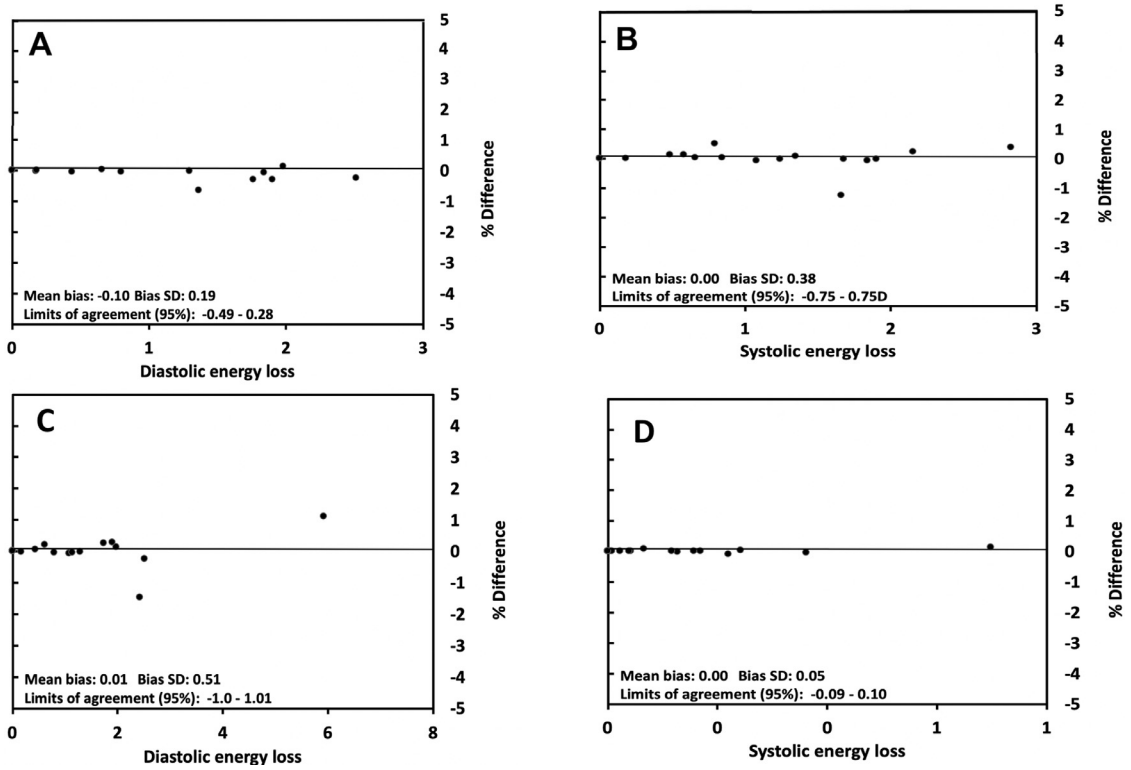

Fig. 7. Bland–Altman plots of intra-observer (A,B) and inter-observer (C, D) agreement. Intra-observer (A,B) and inter-observer (C,D) variability in diastolic and systolic energy loss. In these Bland–Altman plots, the *solid line* represents the average measurement error as a percentage. The calculated mean bias and limits of agreement are displayed in the lower left corner of each graph. The average error in measurement in all cases is well below 5%. SD = standard deviation.

seen and could stem from translational motion of the heart or slight variation of imaging planes (Fig. 6). Computer simulation analysis of the velocity and EL measurements in a ventricular model highlighted some determinants of measurement errors, among which the most important is the alignment with blood flow, but also post-processing settings (*e.g.,* smoothing). Because the postprocessing steps are not major sources of variability, as highlighted by excellent inter- and intraobserver variability, careful and consistent imaging technique become a very important prerequisite for useful and accurate quantitative measures such as energy loss and vorticity in 2-D views. The computer simulation analysis also revealed that diastolic EL was reliable when assessed from a 4CV, as we did here.

Our data indicate that volume-loaded RVs in both rTOF and ASD patients have higher energy losses in diastole compared with those in controls, without being different from each other. In diastole, energy loss occurred at the tricuspid valve leaflets for all groups. This can be understood from a fluid mechanics perspective by the mechanical EL as a result of sudden flow expansion, as it is thought to apply to EL in the ascending aorta of patients with aortic stenosis (Binter et al. 2017). In our study, this sudden flow expansion occurs in early diastole through the tricuspid valve and would be accentuated when the RV is dilated. These findings would support the notion that dilated RVs are less efficient than non-dilated RVs because more kinetic energy is lost during diastole. These findings are in keeping with earlier observations in volume-loaded RVs in a canine study finding reduced diastolic vortex strength and extent, which are quantitative vortical measures thought to correlate with kinetic energy (Pasipoularides et al. 2003).

Even though total diastolic EL was similar in both ASD and rTOF, the two groups exhibited different diastolic flow patterns. In all groups, the tricuspid leaflets were regions of disturbed flow and higher EL. In rTOF, however, an additional region of high EL is present in most cases at the RV apex, associated with colliding flow from the inflow and the PI. These abnormal flow patterns and energetics within the RV apex of rTOF may have effects on remodeling and function. Apical dysfunction has been found to preferentially affect rTOF compared with equally volume-loaded ASD and healthy controls (van der Ven et al. 2019).

In systole, EL did not differ between the groups. This finding was surprising because more energy loss would be expected in rTOF and ASD as the RV stroke volume is increased in these patients compared with controls. The absence of a difference could be attributed to the mostly out-of-plane direction of blood flow in systole when the RV is imaged from the RV4C view. This stems from a well-known and important limitation of 2-D echocardiography in imaging the RV (Haddad et al. 2008).

Contrary to previous studies on flow characteristics and energy loss in children, we could not find a significant correlation between EL and BSA (Hayashi et al. 2015). This explains why EL is expressed as an unindexed measurement in our results. Although systolic EL and diastolic EL did significantly correlate with age in rTOF and CTL, the distribution of EL, especially in older patients, is very wide, and this relationship was not observed in the ASD group. A generalizable conclusion with such data would require more patients.

In addition, the velocity measurements we presented were obtained by blood speckle tracking based on high-frame-rate echocardiography without flow regularization and thus are free of any regularizing assumptions (*e.g.,* without out-of-plane flow). As opposed to techniques such as VFM, wall velocities are not needed to derive any component of the velocity of the blood. The trade-off is dealing with regions of signal dropout as in color Doppler. Two-dimensional energy loss measurements change for physiologic reasons, but also because of variations in the imaging plane and postprocessing settings. As seen from the computer simulation analysis, the wall filter had an overall dampening effect leading to some underestimation of EL, but also changed the curve shape in mid-to-late diastole. The latter could potentially be masking contributing secondary flow patterns and requires further elucidation.

The effect of flow patterns on cardiac morphology and function is complex (Pasipoularides 2012, 2013). Increased fluid shear stress is thought to affect endocardial signaling pathways involved in cardiac remodeling and function (Tseng et al. 1995; Ueba et al. 1997). Disturbances in flow dynamics have been proposed to precede morphologic and functional changes (Pedrizzetti et al. 2015). To study this in the repaired tetralogy of Fallot population, longitudinal changes in flow dynamics and their relationship to RV wall mechanics could be studied. This could provide novel insights into the relationship between flow dynamics and RV remodeling. Energy-based imaging biomarkers are increasingly becoming available based on advancements in MRI and ultrasound technologies (Hirtler et al. 2016; Azarine et al. 2019). Their clinical utility will have to be determined based on longitudinal studies and outcome data. These flow dynamics could reflect RV dysfunction at an earlier, adaptive stage after tetralogy of Fallot repair that would otherwise have been missed using the current imaging biomarkers used. The lack of difference between ASD and rTOF could be related to the small sample size but also reveals the additional value of not only quantitative data of EL and VO, but also qualitative visualization tools allowing differentiation of flow

dynamics between these two groups of volume-loaded RVs. The lack of difference in systolic EL between the groups was a surprising finding. This could again be related to the small sample volume but is more likely explained by the fact the measurements were obtained from a RV4C view, in which systolic flows from the apex to the outlet are largely out of plane. This further indicates the importance of 3-D methods, especially in the setting of complex geometry of the RV.

LIMITATIONS

There were several limitations to this study. The first is the small sample size. The availability of the blood speckle tracking imaging technique only for higher-frequency probes precluded inclusion of older and larger children. This study is to be considered a pilot study hinging on feasibility, validation and potential clinical application of this novel imaging technology.

Acquisition of an RV3C view proved challenging, particularly in healthy controls, in whom the RV is not dilated. However, the RV4C view was more feasible, and we excluded no images in this view. On the basis of results from the validation, we found that it was important to compare images with the same imaging plane to obtain reliable EL and vorticity measurements. Therefore, we chose to exclude 22 of 57 RV3C views with slight differences in angulation. This limitation was compounded by the absence of real-time EL visualization on the modified research scanner used for this study. This meant that quality control was performed offline with no possibility of optimization. As with other Doppler-based techniques of blood flow measurements, multiple acquisitions are analyzed to optimize alignment with the blood flow direction. Similarly, velocities obtained by blood speckle tracking based on high-frame-rate echocardiography will benefit from real-time visualization and analysis.

Another limitation is the 2-D nature of the imaging technique, thus not accounting for through-plane variations. This is highlighted in the systolic EL scatterplots with many values near zero when assessed in the RV4C view (Fig. 2). Because of the crescent shape of the RV, the imaging plane of the RV4C view is nearly perpendicular to the direction of systolic flow toward the outflow tract so that the through-plane component of systolic RV flow is lost.

Calculations of EL are dependent on smoothing parameters. We used the same parameters across our analysis to avoid this potential source of error. However, awareness of this limitation is important for longitudinal studies and for comparison of patient groups in the future.

CONCLUSIONS

Diastolic energy losses in the dilated RVs of patients with ASD and rTOF were similar but significantly higher than in healthy controls, whereas losses were similar in systole. This may support the notion that the dilated RV is less efficient as more energy is lost in diastole (Jeong et al. 2015). In addition, we have found a unique pattern of diastolic energy loss in rTOF within the RV apex, which was not present in the other groups. Colliding jets of pulmonary regurgitation and tricuspid inflow at the RV apex in rTOF are at the origin of this specific pattern. Even though the clinical significance of our findings is not yet clear, the study of disturbances in RV flow and energy loss patterns may provide additional insights into the origin of apical dysfunction seen in the dilated RV of rTOF patients but not ASD. Because no relationship between RV flow dynamics and RV function or mechanics was determined, the link between the two is speculative.

The use of blood speckle tracking for blood flow EL and vorticity quantification proved feasible, with low inter- and intra-observer variability. However, computer simulation validation in this study highlights important aspects related to image acquisition and postprocessing, which can affect the accuracy of the measured blood speckle velocities and EL. Awareness of these limitations is important for future studies and will likely be minimized by the availability of real-time visualization and analysis. High-frame-rate ultrasound and blood speckle tracking are promising new tools in gaining a further understanding of flow dynamics and energetics and their effect on cardiac remodeling and function.

Acknowledgments—We acknowledge the contributions of Guillermo Larios, Wei Hui, Alex Cotoi and Cameron Slorach. We also thank Øyvind Salvesen for advice on the choice of statistical methods.

Conflict of interest disclosure—Exclusive use of a modified GE Vivid E9 was provided by GE during the study period at both institutions. W. M. received funding for this project from the Centre for Innovative Ultrasound Solutions. S.A.N. has funding to this project from the Joint Research Committee between St. Olav's Hospital and the Faculty of Medicine, NTNU, which manages research funding from the Central Norway Regional Health Authority (Reference 2014/23203). Technical development was funded by the Research Council of Norway under RCN 230455 and RCN 237887, the latter through the Centre for Innovative Ultrasound Solutions.

L.L. has a part-time consultancy at GE Vingmed Ultrasound. The other authors have no conflicts of interest to declare.

SUPPLEMENTARY MATERIALS

Supplementary material associated with this article can be found in the online version at doi:10.1016/j.ultrasmedbio.2021.02.004.

REFERENCES

Akiyama K, Maeda S, Matsuyama T, Kainuma A, Ishii M, Naito Y, Kinoshita M, Hamaoka S, Kato H, Nakajima Y, Nakamura N, Itatani K, Sawa T. Vector flow mapping analysis of left ventricular energetic performance in healthy adult volunteers. BMC Cardiovasc Disord 2017;17:21. Erratum: BMC Cardiovasc Disord 2017;17:172.

Azarine A, Garcon P, Stansal A, Canepa N, Angelopoulos G, Silvera S, Sidi D, Marteau V, Zins M. Four-dimensional flow MRI: Principles and cardiovascular applications. Radiographics 2019;39:632–648.

Binter C, Gotschy A, Sündermann SH, Frank M, Tanner FC, Lüscher TF, Manka R, Kozerke S. Turbulent kinetic energy assessed by multipoint 4-dimensional flow magnetic resonance imaging provides additional information relative to echocardiography for the determination of aortic stenosis severity: Clinical perspective. Circ Cardiovasc Imaging 2017;10 e005486.

Dragulescu A, Grosse-Wortmann L, Redington A, Friedberg MK, Mertens L. Differential effect of right ventricular dilatation on myocardial deformation in patients with atrial septal defects and patients after tetralogy of Fallot repair. Int J Cardiol 2013;168:803–810.

Dragulescu A, Friedberg MK, Grosse-Wortmann L, Redington A, Mertens L. Effect of chronic right ventricular volume overload on ventricular interaction in patients after tetralogy of Fallot repair. J Am Soc Echocardiogr 2014;27:896–902.

Fadnes S, Wigen MS, Nyrnes SA, Lovstakken L. In vivo intracardiac vector flow imaging using phased array transducers for pediatric cardiology. IEEE Trans Ultrason Ferroelectr Freq Control 2017;64:1318–1326.

Fogel MA, Sundareswaran KS, De Zelicourt D, Dasi LP, Pawlowski T, Rome J, Yoganathan AP. Power loss and right ventricular efficiency in patients after tetralogy of Fallot repair with pulmonary insufficiency: Clinical implications. J Thorac Cardiovasc Surg 2012;143:1279–1285.

Haddad F, Hunt SA, Rosenthal DN, Murphy DJ. Right ventricular function in cardiovascular disease: Part I. Anatomy, physiology, aging, and functional assessment of the right ventricle. Circulation 2008;117:1436–1448.

Hayashi T, Itatani K, Inuzuka R, Shimizu N, Shindo T, Hirata Y, Miyaji K. Dissipative energy loss within the left ventricle detected by vector flow mapping in children: Normal values and effects of age and heart rate. J Cardiol 2015;66:403–410.

Hirtler D, Garcia J, Barker AJ, Geiger J. Assessment of intracardiac flow and vorticity in the right heart of patients after repair of tetralogy of Fallot by flow-sensitive 4 D MRI. Eur Radiol 2016;26:3598–3607.

Jeong D, Anagnostopoulos PV, Roldan-Alzate A, Srinivasan S, Schiebler ML, Wieben O, François CJ. Ventricular kinetic energy may provide a novel noninvasive way to assess ventricular performance in patients with repaired tetralogy of Fallot. J Thorac Cardiovasc Surg 2015;149:1339–1347.

Nakashima K, Itatani K, Kitamura T, Oka N, Horai T, Miyazaki S, Nie M, Miyaji K. Energy dynamics of the intraventricular vortex after mitral valve surgery. Heart Vessels 2017;32:1123–1129.

Nyrnes SA, Fadnes S, Wigen MS, Mertens L, Lovstakken L. Blood speckle tracking based on high frame rate ultrasound imaging in pediatric cardiology. J Am Soc Echocardiogr 2020;33 493−503.e5.

Pasipoularides A. Diastolic filling vortex forces and cardiac adaptations: Probing the epigenetic nexus. Hell J Cardiol 2012;53:458–469.

Pasipoularides A. Evaluation of right and left ventricular diastolic filling. J Cardiovasc Transl Res 2013;6:623–639.

Pasipoularides A, Shu M, Shah A, Womack MS, Glower DD. Diastolic right ventricular filling vortex in normal and volume overload states. Am J Physiol Heart Circ Physiol 2003;284:H1064–H1072.

Pedrizzetti G, Martiniello AR, Bianchi V, D'Onofrio A, Caso P, Tonti G. Cardiac fluid dynamics anticipates heart adaptation. J Biomech 2015;48:388–391.

Shibata M, Itatani K, Hayashi T, Honda T, Kitagawa A, Miyaji K, Ono M. Flow energy loss as a predictive parameter for right ventricular deterioration caused by pulmonary regurgitation after tetralogy of Fallot repair. Pediatr Cardiol 2018;39:731–742.

Tseng H, Peterson TE, Berk BC. Fluid shear stress stimulates mitogen-activated protein kinase in endothelial cells. Circ Res 1995;77:869–878.

Ueba H, Kawakami M, Yaginuma T. Shear stress as an inhibitor of vascular smooth muscle cell proliferation. Arterioscler Thromb Vasc Biol 1997;17:1512–1516.

Van Cauwenberge J, Lovstakken L, Fadnes S, Rodriguez-Morales A, Vierendeels J, Segers P, Swillens A. Assessing the performance of ultrafast vector flow imaging in the neonatal heart via multiphysics modeling and *in vitro* experiments. IEEE Trans Ultrason Ferroelectr Freq Control 2016;63:1772–1785.

van der Ven JPG, van den Bosch E, Bogers AJCC, Helbing WA. Current outcomes and treatment of tetralogy of Fallot. F1000Research 2019;8:1530.

Wigen MS, Fadnes S, Rodriguez-Molares A, Bjastad T, Eriksen M, Stensæth KH, Støylen A, Lovstakken L. 4-D intracardiac ultrasound vector flow imaging—Feasibility and comparison to phase-contrast MRI. IEEE Trans Med Imaging 2018;37:2619–2629.

Zhong Y, Liu Y, Wu T, Song H, Chen Z, Zhu W, Cai Y, Zhang W, Bai W, Tang H, Rao L. Assessment of left ventricular dissipative energy loss by vector flow mapping in patients with end-stage renal disease. J Ultrasound Med 2016;35:965–973.